Study of the local field distribution on a single-molecule magnet–by a single paramagnetic crystal; a DPPH crystal on the surface of an Mn_{12}-acetate crystal

Dijana Žilić[a], Boris Rakvin[a], Naresh S. Dalal[b]

[a]*Department of Physical Chemistry, Ruđer Bošković Institute,*
Bijenička cesta 54, 10000 Zagreb, Croatia
[b]*Department of Chemistry and Biochemistry, Florida State University,*
Tallahassee, FL 32306, USA

Abstract

The local magnetic field distribution on the subsurface of a single-molecule magnet crystal, SMM, above blocking temperature ($T >> T_b$) detected for a very short time interval ($\sim 10^{-10}$ s), has been investigated. Electron Paramagnetic Resonance (EPR) spectroscopy using a local paramagnetic probe was employed as a simple alternative detection method. An SMM crystal of $[Mn_{12}O_{12}(CH_3COO)_{16}(H_2O)_4] \cdot 2CH_3COOH \cdot 4H_2O$ (Mn_{12}-acetate) and a crystal of 2,2-diphenyl-1-picrylhydrazyl (DPPH) as the paramagnetic probe were chosen for this study. The EPR spectra of DPPH deposited on Mn_{12}-acetate show additional broadening and shifting in the magnetic field in comparison to the spectra of the DPPH in the absence of the SMM crystal. The additional broadening of the DPPH linewidth was considered in terms of the two dominant electron spin interactions (dipolar and exchange) and the local magnetic field distribution on the crystal surface. The temperature dependence of the linewidth of the Gaussian distribution of local fields at the SMM surface was extrapolated for the low temperature interval (70–5 K).

Keywords: Mn_{12}-acetate, DPPH, EPR

1. Introduction

Single-molecule magnets (SMMs) are candidates for many applications, such as quantum computation, high-density magnetic data storage and magnetoelectronics [1, 2]. In order to develop these applications, it is important to investigate what happens when they are in contact with other dissimilar materials, as it is expected that their wave functions and/or magnetic fields extend considerably outside the physical structure [3]. This also implies improved detection of the magnetic fields on their surfaces *i. e.*, the magnetic field generated by a crystal in the vicinity of its surface. The magnetic properties of SMMs at temperatures above blocking temperature, $T > T_B$, can be considered as superparamagnetic properties. The relaxation of magnetization in this temperature region can be described by the Arrhenius law $M(t) = M_0 \exp(-t/\tau)$, with a characteristic relaxation time, τ [4]. Such a relaxation time in the simple form is given as a function of the energy barrier, E_b, and temperature ($\tau = \tau_0 \exp(E_b/kT)$). When a magnetic field is applied, the total energy barrier is expected to be lower [4]. Thus, at the surface of the SMM crystal one expects time-dependent as well as magnetic-field-dependent distribution of the magnetic fields. In superparamagnetic systems, the observed magnetic behavior strongly depends on the value of the measuring time, t_m, of the employed experimental technique with respect to intrinsic τ. Therefore, wide variation can be expected in the employed time "window"-which varies from large values as in magnetization measurements (typically 100 s) to very small ones, as in ac susceptibility [5] or spectroscopy [6] (10^{-8} s). The detection and description of such distributions of local fields at the surface as functions of the orientation of the SMM crystal in the external magnetic field within a very short time interval ($\sim 10^{-10}$ s) are the focus of the present study.

Electron Paramagnetic Resonance (EPR) spectroscopy with a local paramagnetic probe will be employed as an alternative simple detection method. As shown recently [6, 7, 8], an EPR technique in combination with several characteristic paramagnetic probes shows a reliable capability for such measurements for the most common EPR spectrometers involving magnetic field ~0.35 T with corresponding X-band

frequency (~9.5 GHz). An additional characteristic of this detection is related to the possibility of deducing a time-dependent fluctuation of the local field in a short time scale [6]. In the previous studies, the probes used were a powder of 2,2-diphenyl-1-picrylhydrazyl (DPPH) and needle-shaped N-methylphenazinium-tetracyanoquinodimethane (NMP-TCNQ). The EPR spectrum of the powder (DPPH grains < 1 μm) shows very narrow singlet lines with peak-to-peak linewidth, W_{pp} ~0.15 mT, having an almost constant g-value in a wide temperature range from room temperature down to that of liquid helium. On the other side, DPPH powder spread on the restricted surface of the SMM crystal shows a broad EPR spectrum around the resonance field, B_0, with characteristic shoulders in the low temperature region (4–100 K) [7]. Such a spectrum represents a proportional "fingerprint" of the expected field distributions at the area of the SMM crystal surfaces covered by the probe. The relaxation of SMM magnetization in the low temperature region (4–50 K) is significantly slower than the detection time of EPR spectroscopy ($\tau \gg t_m$) [9, 10]. Thus, the effect of magnetic-field fluctuation will be detected as the distribution of nearly static magnetic field components. It was shown earlier [7, 8] that the characteristic shoulders of the complex powder spectrum of the probe depend on the SMM orientation in the magnetic field. These shoulders exhibited temperature-dependent shifts, which correlated with SQUID measured magnetization of the SMM for the givens orientation in the magnetic field. However, there is a weakness in the detection of the shoulders, particularly for the largest shift, since its intensity significantly decreases, below the limit of spectrometer signal-to-noise ratio at low temperatures. In order to improve the sensitivity of the method, a DPPH crystal is considered as a better probe for the detection of the local shift as well as the monitored distribution of the local fields. It is expected that due to the presence of the fast electron spin exchange interaction inside the DPPH crystal, the broad distribution of the local fields at the surface of the SMM will be averaged into a single line. In addition, it is expected that the obtained singlet will be broader than the singlet of DPPH in the absence of the SMM crystal. In the present work, the possibility of using a crystal of DPPH as a local probe on the surface of the most frequently investigated SMM, Mn$_{12}$-acetate, [Mn$_{12}$O$_{12}$(CH$_3$COO)$_{16}$(H$_2$O)$_4$]·2CH$_3$COOH·4H$_2$O (hereafter abbreviated as Mn12), will be investigated and discussed.
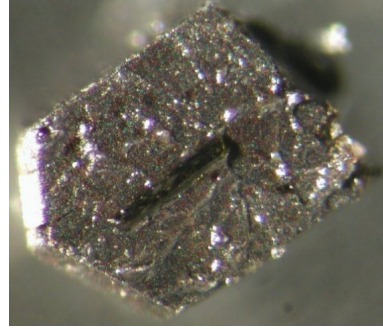

Figure 1: (Color online.) DPPH single crystal mounted by vacuum grease on the surface of an Mn12 single crystal, shown under ~ 20× magnification. The a axis of the DPPH was parallel to the z axis of the Mn12.

2. Experimental

Single crystals of Mn12 were grown using Lis' procedure [11], and grew into rectangular rods of a few mm^3 in dimension. The easy axis of magnetization, the z axis, was along the longest dimension of the crystals. Single crystals of DPPH were crystallized from a solution of DPPH in ether using the procedure described in [12]. The dimensions of the DPPH crystals were approximately $1 \times 0.2 \times 0.2$ mm^3. The crystals of DPPH were elongated along the crystallographic a axis. The DPPH crystal was fixed by using vacuum grease on the Mn12 crystal, as shown in Fig. 1.

EPR measurements were carried out with a Bruker 580 FT/CW X-band EPR spectrometer equipped with a standard Oxford Instruments Model DTC2 Temperature Controller (4–300 K). All the measurements were performed with a magnetic field modulation amplitude of ~ 5 μT at 100 kHz.

3. Results and discussion

The EPR spectra of the single crystal of the DPPH probe at various orientations in the magnetic field exhibit a narrow Lorentzian profile of a detected singlet with an average g-value of g = 2.004 ± 0.001 and peak-to-peak linewidths of W_{pp} = (0.15 ± 0.03) mT, in the wide temperature range 4–300 K [12]. The DPPH crystal was deposited on the Mn12 crystal with selected orientation, as shown in Fig. 1. The a axis of the DPPH crystal was oriented parallel to the z axis of the Mn12 (along the easy axis of the Mn12). At room temperature, the probe mounted on the Mn12 crystal shows approximately the same spectra as the probe itself at the resonance field, B_0. In the process of lowering the temperature, the EPR line of the probe deposited on the
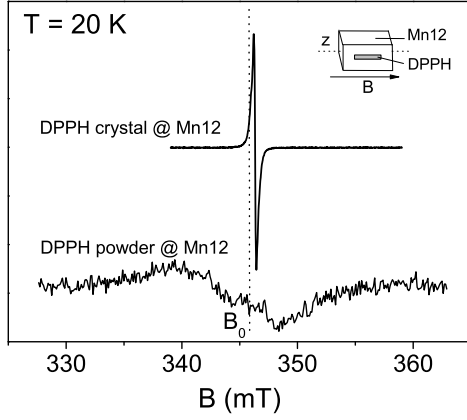
Figure 2: The EPR spectra of DPPH powder and a DPPH single crystal deposited on the surface of an Mn12 crystal, at T = 20 K. The magnetic field was parallel to the easy axis of Mn12 ($B \parallel z$). The dashed line represents the resonant field, B_0, for both DPPH samples (without Mn12).

Figure 3: The EPR spectra of the DPPH single crystal deposited on the surface of the Mn12 crystal, at T = 5 K. The spectra were recorded for a different angle, θ, between magnetic field B and the z axis of the Mn12 crystal, in steps of 5°. The dashed line represents the resonant field, B_0, for the DPPH single crystal (without Mn12).

Mn12 broadened and shifted from the resonance position B_0. Fig. 2 illustrates significant differences in the spectra between the powder and crystal DPPH deposited on the Mn12 crystal and detected in the low temperature region (at 20 K). One should note that the broad powder spectrum appeared from both sides of the B_0 in contrast to the sharp crystal spectrum, which exhibited a clear shift from the B_0.

The EPR spectra for a different angle θ between magnetic field B and easy axis z, are shown in Fig. 3.

In the case when $\theta = 0°$, the detected spectral line was shifted in the direction to a higher magnetic field, in comparison to the B_0. For the perpendicular orientation of the magnetic field ($\theta = 90°$) the line is shifted in the opposite direction of the B_0. Between these two canonical orientations, the spectral line exhibited an additional splitting structure, as shown in Fig. 3. The results obtained significantly differ from a similar experiment in which a DPPH crystal was replaced by DPPH powder.

As was demonstrated in Fig. 2 and in a series of earlier experiments [7], a powder probe exhibits a broad spectrum, with a pattern that contains characteristic shoulders. As also shown earlier [7], these shoulders are scaled with SQUID measured magnetizations (for two orientations: $B \parallel z$ and $B \perp z$) in the same temperature interval. The same procedure was applied on measured shifts for each orientation of the Mn12 crystal labeled with a crystal probe. Indeed, the field shift of the crystal probe for the corresponding orientation of the Mn12 crystal shows proportionality with independently mea-
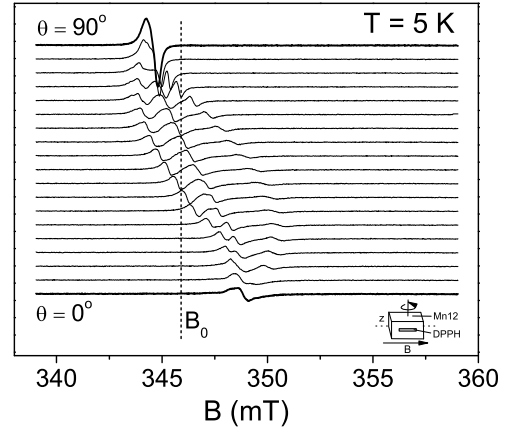
sured SQUID magnetizations [7], as shown in Fig. 4.

From a good match of EPR and SQUID data in Fig. 4, it is obvious that additional magnetic field "experienced" by the probes has the origin in the magnetization of Mn12. Larger shift for $B \parallel z$ compared to $B \perp z$ is due to much larger component of magnetization along the easy axis of Mn12 compared to the hard axis. From the Fig. 4 it could be seen that magnitude of the averaged field shift for the probe at the surface of Mn12 is ~1 mT at low temperature.

In order to reveal the microscopic origin in the difference between the crystal and DPPH powder deposited on the Mn12 crystal, it was noted that different orientations of DPPH crystal on the surface, for the same Mn12 crystal orientation in the magnetic field, showed nearly the same shift of the spectrum line. Thus, the results obtained support the above-mentioned expectation that a wide distribution of local fields at the surface of the Mn12 crystal is averaged out by the crystal probe (DPPH crystal). At the same time, the "long range" of the exchange interaction with an averaging behavior is absent for the powder probe. A further consequence of this experiment is that the "shorter range" of the spin-spin type of exchange interaction in powder grains than in the crystal continuum emerges as the only possible difference between the powder and crystal probe. It is expected that a small particle within the powder could only partly average local fields and finely a broad spectrum with characteristic powder pat-
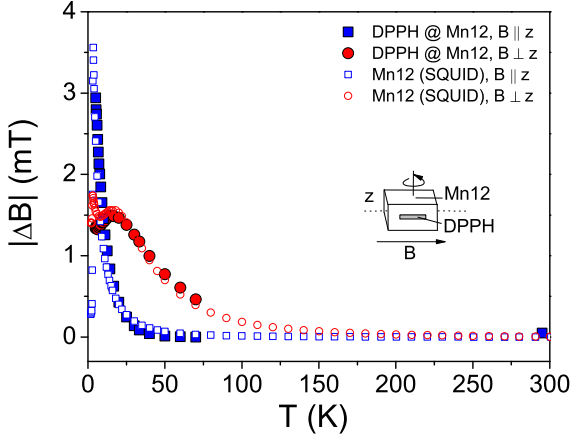
Figure 4: (Color online.) Comparison of EPR and SQUID magnetization data. Temperature variation of the effective magnetic field "experienced"by probes (DPPH crystal) on the surface of Mn12 measured by EPR (filled symbols) compared with the scaled SQUID magnetization (open symbols).

Table 1: Experimental and calculated parameters of linewidths for the DPPH crystal with and without the Mn12 crystal, at 10 K. All the quantities are expressed in mT.

W_{pp0}	W_{pp}	Γ_{d0}	H_{exch}	Γ_d
0.14	0.21	19.5	3142.8	23.9

tern is obtained. Additional important evidence should be noted from the present experiment. Since, the exchange interaction is expected to predominate on the level of the DPPH molecule pairs [12, 13], the distribution of the local fields is expected to exhibit space inhomogeneity (with possible variation of the gradient) at comparable distances. Such local fields with space inhomogeneity at ~1 nm scale are indeed expected for Mn12 in the superparamagnetic state.

The nature of DPPH spectra (in the powder or crystal form) is related to two dominant spin-spin interactions: dipole-dipole and exchange interaction. A spin dipole-dipole interaction is proportional to $1/a^6$ (where a is the distance between molecules) and contributes significantly to the broadening of the resonance line since an unpaired electron spin density is present at each DPPH molecule in the crystal. It is also known that such broadening of the resonance line (assuming a Gaussian line shape) could be approximated with the square root of the second moment of the resonant line, M_2 [14]. In order to evaluate the M_2 of DPPH ($S = 1/2$), approximation calculus for a powder sample with cubic symmetry was employed [15]. The second moment is additionally averaged over a sphere for spin i to yield:

$$M_2 = \frac{10}{3}\frac{3}{5}g^2\beta^2 S(S+1)\sum_j r_{ij}^{-6}. \qquad (1)$$

Here, the term $i = j$ is excluded from the summation and the symbols have their usual meanings. The factor 10/3

(the so-called "10/3" effect) is added because of subsidiary lines that appear at $\sim 0, 2g\beta H$ and $3g\beta H$ [15]. Considering the contribution of the nearest molecules for the sphere of a radius of 15 Å, the corresponding dipolar contribution to the DPPH linewidth, Γ_{d0}, has been calculated:

$$\Gamma_{d0} \approx \sqrt{M_2}. \qquad (2)$$

where Γ_{d0} is the half-width at half-intensity and is given in Table 1.

Thus, the spin dipole-dipole contribution leads to a relatively broad spectrum, which is two orders of magnitude broader than the experimental linewidth value of DPPH ($\Gamma_{d0} >> W_{pp0}$). The linewidths for the DPPH crystal with and without Mn12, W_{pp} and W_{pp0}, respectively, are given in Table 1. The experimental spectral lines of the probes showed approximately Lorentzian shapes, and the following could be written for the effective Lorentzian linewidths [16]:

$$\Gamma_{L0} = \sqrt{3}/2W_{pp0}. \qquad (3)$$

In the case when the exchange interaction is strong, the orientation of neighboring spins is exchanged at the rate of order of H_{exch} through mutual spin flips so that the local dipolar field fluctuates at similar rate and tends to average out. In the case if $H_{exch} >> \Gamma_{d0}$, the broad line shape becomes nearly Lorentzian with an approximate half-width [15]:

$$\Gamma_{L0} \approx (\Gamma_{d0})^2/H_{exch}. \qquad (4)$$

Relation 4 and the data in Table 1 can be used to estimate H_{exch} for the DPPH crystal. The value obtained is given in Table 1 (H_{exch} = 3142.8 mT ~ 4.2 K) and is in good agreement with earlier deduced values for the exchange constant of DPPH [12]. If the DPPH crystal is deposited on the Mn12 crystal, the local dipolar field of the DPPH molecule increases by the contribution of the local Mn12 fields and the same exchange interaction will reduce both dipolar contributions, Γ_d, in an effectively Lorentzian line shape with a peak-to-peak linewidth, W_{pp}. For experimentally measured W_{pp} one simply calculates the Γ_d value, given in Table 1 (as in relation 4). It is easy to obtain ($\Delta\Gamma_d = \Gamma_d - \Gamma_{d0}$ = 4.4 mT),
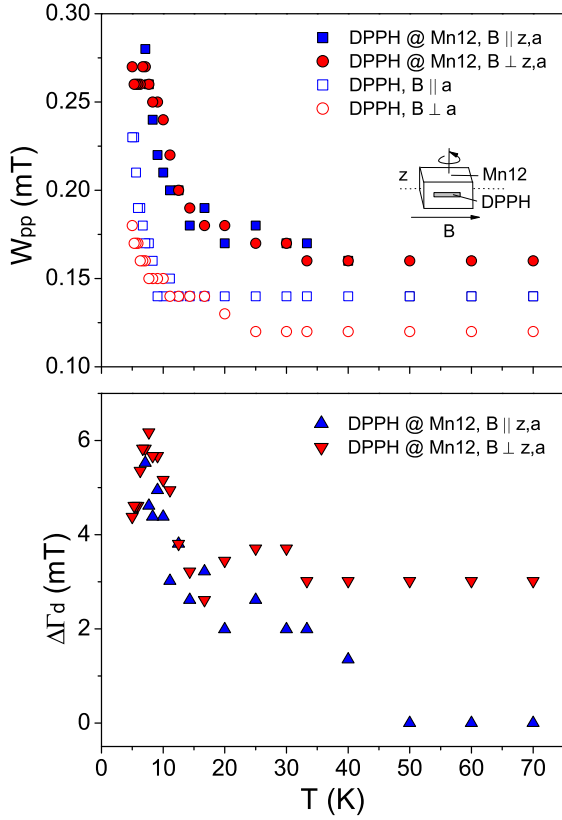
4

Figure 5: (Color online.) *Upper:* Experimentally obtained temperature variation of linewidths for DPPH (open symbols) and for DPPH deposited on Mn12 (filled symbols). *Lower:* The calculated temperature dependence of the dipolar field, $\Delta\Gamma_d$, caused by the Mn12 crystal at the position of the DPPH crystal, according to relation 5.

the average dipolar field being caused by the presence of the Mn12 crystal. This value also represents an average distribution of the local fields on the surface of the Mn12 crystal at the position of the DPPH crystal. The same procedure was applied for the estimation of the linewidth of the Gaussian distribution of the local fields measured on the surface of the Mn12 crystal at the position of the DPPH crystal in a wide temperature interval (Fig. 5):

$$\Delta\Gamma_d = \Gamma_{d0}(\sqrt{W_{pp}/W_{pp0}} - 1). \quad (5)$$

Generally, these values indicate increases with decreasing temperature in the monitored region of low temperatures. At this moment, the corresponding activation process with the approximate activation energy $\sim$ 10 K could not be simply correlated with one of microscopic parameters known for the Mn12 crystal

[9, 10]. It is also important to note that the obtained value of the Gaussian distribution of the local fields coincides with the linewidth of the broad spectrum of DPPH powder within an order of magnitude. This provides additional indication that the "long range" spin-spin exchange interaction present in the crystal is involved in the narrowing of the local field distribution.

4. Conclusions

A DPPH crystal as a probe shows several advantages in respect to a DPPH powder probe for detecting the distribution of local fields on the surface of an SMM crystal. It is clearly shown that "discontinuity" (or "short range") of exchange interaction significantly contributes to broaden the spectra of a powder probe. This broadening is related to decreasing spectral intensity and lead to uncertainty in the detection of the characteristic spectral shoulders. Thus, temperature-dependent measurements, especially at low temperature at higher local fields, are not possible. On the other side, a crystal probe, due to the presence of exchange interaction on the longer range scale than in powder, efficiently averages all the local fields within the crystal, resulting in a narrow Lorentz-type line around the center of distribution, as seen in Fig. 2. The narrowing helps to estimate the shift of the spectral line more accurately, even in the low temperature region. With this method, accuracy is particularly improved for the detection of the average distribution of the local fields in the form of the linewidth of the Gaussian distribution. As shown above, this accuracy is closely related to the accuracy of the exchange constant of the probe. It should also be mentioned that the behavior of the exchange interactions within organic-type paramagnetic crystals is not known in detail. It is expected that these exchange interactions depend on various microscopic models of exchange between the paramagnetic molecules in the crystal, leading to possible exchange distribution within the crystal continuum. Indications for such symmetry-dependent distribution of the exchange interaction within the crystal are present in the splitting spectra of the DPPH probe when the magnetic field was neither parallel nor perpendicular to the easy axis of Mn12 (Fig. 3). This characteristic of the exchange interaction has also been noted for other organic crystal probes, the DPPH crystal–containing solvent molecule (CS_2) [12], the α,γ-bisdiphenylene-β-phenylallyl (BDPA) crystal and the previously studied TCNQ poly-crystal [6, 8]. Thus, SMM crystals with a broad distribution of local fields at the surface that exhibit space inhomogeneity at the nano scale could be

used as possible devices for the investigation of the exchange interaction in organic-type paramagnetic crystals. Indeed, such an application of SMM is under investigation and the results obtained will be discussed and published elsewhere.

Acknowledgments

[1] M. N. Leuenberger and D. Loss, Nature **410**, 789 (2001).

[2] M. N. Leuenberger, F. Meier, and D. Loss, Monatshefte für Chemie / Chemical Monthly **134**, 217 (2003).

[3] J. Eisenmenger and I. K. Schuller, Nat. Mater. **2**, 437 (2003).

[4] D. Gatteschi, R. Sessoli, and J. Villain, *Molecular Nanomagnets* (Oxford University Press, Oxford, UK, 2006).

[5] R. Blinc *et al.*, Phys. Rev. B **67**, 094401 (2003).

[6] B. Rakvin, D. Žilić, and N. S. Dalal, Solid State Commun. **136**, 518 (2005).

[7] B. Rakvin *et al.*, Spectrochim. Acta A **60**, 1241 (2004).

[8] B. Rakvin, D. Žilić, J. M. North, and N. S. Dalal, J. Magn. Reson. **165**, 260 (2003).

[9] R. Sessoli, D. Gatteschi, A. Caneschi, and M. A. Novak, Nature **365**, 141 (1993).

[10] M. A. Novak, W. S. D. Folly, J. P. Sinnecker, and S. Soriano, J. Magn. Magn. Mater. **294**, 133 (2005).

[11] T. Lis, Acta Crystallogr. B **36**, 2042 (1980).

[12] D. Žilić *et al.*, J. Magn. Reson. **207**, 34 (2010).

[13] T. Fujito, Bull. Chem. Soc. Jpn. **54**, 3110 (1981).

[14] M. Goldman, *Spin Temperature and NMR in Solids,* (Oxford University Press, UK, 1970).

[15] C. P. Poole, Jr., *Electron Spin Resonance: A Comprehensive Treatise on Experimental Techniques* (John Wiley and Sons, Inc., New York, 1983).

[16] J. A. Weil, J. R. Bolton, and J. E. Wertz, *Electron Paramagnetic Resonance* (John Wiley and Sons, Inc., New York, 1994).